Supplementary Information

Efficient and durable hydrogen evolution electrocatalyst based on nonmetallic nitrogen doped hexagonal carbon

Yanming Liu, Hongtao Yu, Xie Quan*, Shuo Chen, Huimin Zhao & Yaobin Zhang

Department of Chemical, Environmental and Biological Science and Technology, Dalian University of Technology, Dalian 116024, China.

*Corresponding author e-mail: quanxie@dlut.edu.cn

Table S1 Comparison of HER performance of NHC and the non-noble electrocatalysts reported (pH is 0 unless otherwise specified, the catalyst loading of NHC electrode is the loading of TiC and NHC film).

	Onset potential (mV vs. RHE)	Tafel slope (mV dec^{-1})	Exchange current density (mA cm^{-2})	Catalyst loading (mg cm^{-2})	Refs.
Cu_2MoS_4	-135	95	4.0×10^{-2}	0.04	18
Mo_2C/XC (pH 1)	-105	59.4	8.1×10^{-3}	2	16
Mo_2S/Au	-90	69.0	9.3×10^{-3}	-	17
Mo2C	-100	56	1.3×10^{-4}	340	32
MoB	-100	55	1.4×10^{-4}	340	32
$C_{60}(OH)_8$	-110	78	7×10^{-4}	-	20
C_3N_4 (pH 6.9)	-250	-	-	-	19
NHC	-65	56.7	5.7×10^{-2}	< 12.5	This work

NHC electrode is active for HER at pH 7 and pH 14 with an onset potential of -150 mV (Fig. S1), beyond which the cathodic current density increases rapidly under more negative potentials. For driving a current density of 10 mA cm^{-2}, NHC electrode requires an overpotential of 0.32 V at pH 7 and 0.37 V at pH 14. These results indicate NHC electrode is more active for HER at a lower pH value. It is worth noting that NHC is advantageous over the reported carbon nitride[19] for HER at neutral solution in terms of onset potential and cathodic current density (Table S1), suggesting the good performance of NHC electrode for HER at neutral solution.

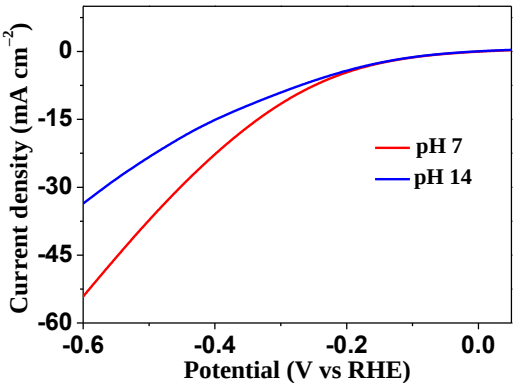

Figure S1 | HER activity of NHC electrode. Linear sweep voltammograms of NHC electrode at pH 7 (0.5 M Na_2SO_4) and pH 14 (1 M KOH) with a scan rate of 5 mV s^{-1}.

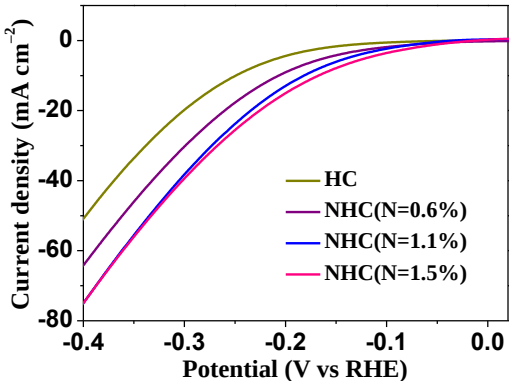

Figure S2 | HER activity of HC and NHC electrodes. Linear sweep voltammograms of HC electrode and NHC electrodes with nitrogen content 0.6 at.%, 1.1 at.% and 1.5 at.% in 0.5 M H_2SO_4 (scan rate 5 mV s^{-1}).

Table S2 The reactant content of different electrocatalysts.

	H_2	CH_4	N_2	sp^2/sp^3	sp^2-C
NHC1	89.2%	10.0%	0.8%	0.49	32.9%
NHC2	84.2%	15.0%	0.8%	0.74	42.5%
NHC3	79.2%	20.0%	0.8%	1.02	50.5%

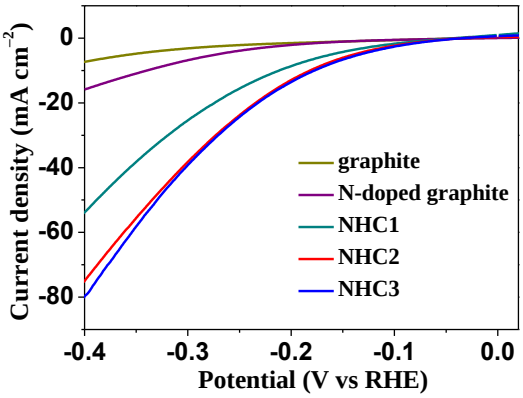

Figure S3 | HER activity. Linear sweep voltammograms of commercial graphite, N-doped graphite (N = 1.5 at.%), NHC1, NHC2 and NHC3 electrodes in 0.5 M H_2SO_4 (scan rate 5 mV s^{-1}).

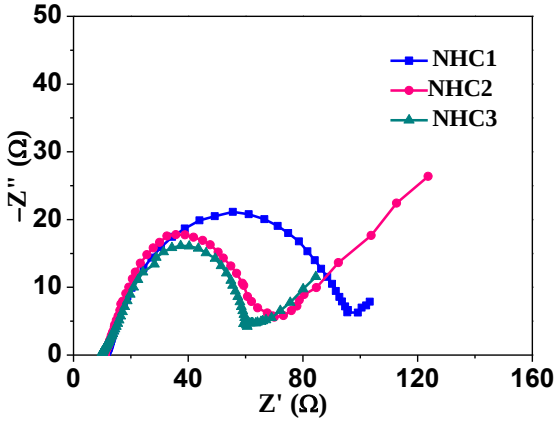

Figure S4 | Comparison of charge-transfer resistances. Nyquist plots of NHC1 (sp^2/sp^3=0.49), NHC2 (sp^2/sp^3=0.74) and NHC3 (sp^2/sp^3=1.02) electrodes in 0.5 M H_2SO_4 solution.

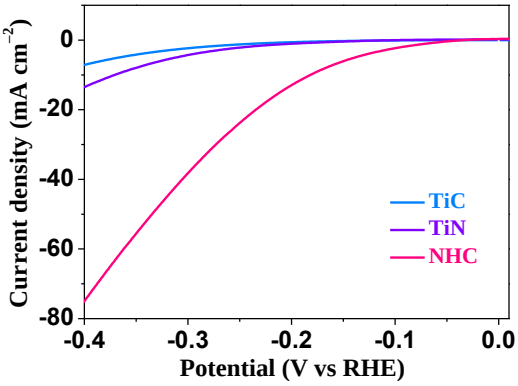

Figure S5 | HER activity. Linear sweep voltammograms of commercial TiC, commercial TiN and NHC electrodes in 0.5 M H_2SO_4 (scan rate 5 mV s^{-1}).

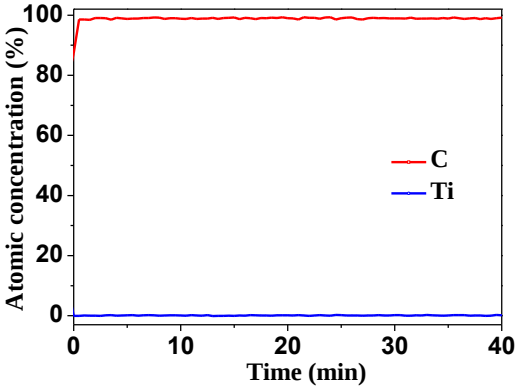

Figure S6 | Auger depth profiles of NHC electrode. The variation of C and Ti atomic concentrations with sputtering time (sputtering rate is about 50 nm/min).

During the entire experiment, the possible source of metal contamination is Ti substrate (99.99%) or chemical vapor deposition chamber (containing stainless steel). Therefore, NHC film has been analyzed by inductively coupled plasma atomic emission spectroscopy (ICP-AES) for the following metals: Ti, Pt, Pd, Au, Ag, Fe, Cu, Co, Cr, Mn, Ni, Mo, Nb, Mg. The samples for ICP-AES analysis were prepared as follows: NHC film (20 mg) was scratched from the Ti substrate and dissolved in a mixture of $HNO_3/HClO_4$ (v/v = 1/1, 5 mL) solution by boiling for 10 h. To minimize measurement error, three samples were prepared. The results show the concentrations of Pt, Pd, Au, Ag, Fe, Cu, Co, Cr, Mn, Ni, Mo, Nb and K are lower than the detection limit. Then we determined the detection limit of these metals by measuring the blank samples. According to their detection limits, the concentrations of Pt, Pd, Au, Ag, Fe, Cu, Co, Cr, Mn, Ni, Mo and Nb are lower than 2.5×10^{-5} wt.%, 3.0×10^{-5} wt.%, 3.0×10^{-5} wt.%, 5.7×10^{-5} wt.%, 7.3×10^{-4} wt.%, 1.7×10^{-4} wt.%, 1.5×10^{-4} wt.%, 8.1×10^{-4} wt.%, 1.2×10^{-4} wt.%, 7.0×10^{-4} wt.%, 7.7×10^{-4} wt.%, 5.9×10^{-4} wt.% and 4.9×10^{-4} wt.% of NHC film, respectively (Table S3). Based on the results of numerous literatures[1-5], the lowest concentrations of metal impurities which are effective for electro-reduction are hundreds of ppm for Fe and Ni, tens of ppm for Co, Cu and Mo, several ppm for Pt. Compared with these concentration levels, the metal (if exists) concentrations of NHC film are much lower, which suggests metal impurities of NHC film have no obvious effect on HER activity. The Ti concentration in sample 1 is also lower than the detection limit, while its concentration in sample 2 and 3 are 0.2024 mg L^{-1} and 0.4370 mg L^{-1}, corresponding to 0.020 wt.% and 0.044 wt.% for NHC film, respectively. To confirm whether the detected Ti was from the Ti substrate or NHC film, XPS was performed to determine the Ti content on the surface of NHC electrode. XPS spectrum shows Ti is not detected on the surface of NHC electrode, but the Ti content in sample 2 and 3 is detectable by XPS. Therefore, the detected Ti should be originated from Ti substrate during scratching because it is difficult for NHC film to exfoliate from Ti substrate without Ti contamination. Besides, Ti exhibits neglectable activity for electrocatalytic HER at –0.4 V ~ 0 V.

Table S3 The metal contents of NHC film determined by ICP-AES

metal	Pt	Pd	Au	Ag	Fe	Cu	Co		
content(wt%)	$\leq 2.5\times10^{-5}$	$\leq 3.0\times10^{-5}$	$\leq 3.0\times10^{-5}$	$\leq 5.7\times10^{-5}$	$\leq 7.3\times10^{-4}$	$\leq 1.7\times10^{-4}$	$\leq 1.5\times10^{-4}$		
metal	Cr	Mn	Ni	Mo	Nb	Mg	Ti		
content(wt%)	$\leq 8.1\times10^{-4}$	$\leq 1.2\times10^{-4}$	$\leq 7.0\times10^{-4}$	$\leq 1.5\times10^{-4}$	$\leq 5.9\times10^{-4}$	$\leq 4.9\times10^{-4}$	$\leq 5.9\times10^{-4}$	0.020	0.044

It has been reported that Pt is favorable for CO adsorption and the adsorbed CO will result in deactivation of Pt. Therefore, to confirm the absence of Pt, linear sweep voltammograms (LSVs) of NHC electrode have been tested before and after CO adsorption. Adsorption of CO at NHC electrode was conducted at potential 0.05 V by bubbling CO into 0.5 M H_2SO_4 for 0.5 h[6]. Then, the LSV of NHC electrode was tested under CO bubbling. After CO adsorption, the HER activity of NHC electrode keeps the same as that without CO (Fig. S7), which suggests that Pt is absence at NHC electrode and the HER activity of NHC electrode is originated from NHC film instead of Pt.

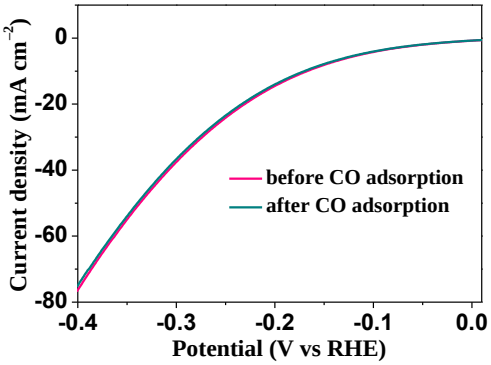

Figure S7 | HER activity of NHC electrode. Linear sweep voltammograms of NHC electrodes before and after CO adsorption in 0.5 M H_2SO_4 (scan rate 5 mV s^{-1}).

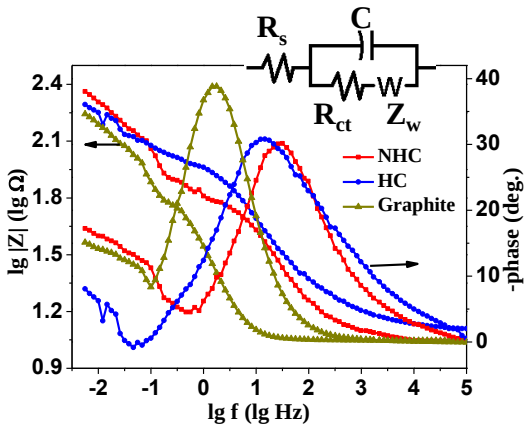

Figure S8 | Bode plots and equivalent circuit model. Bode plots of graphite, HC and NHC electrodes in 0.5 M H_2SO_4 solution. The inset is the equivalent circuit model, R_s is the solution resistance, C is double layer capacitance, R_{ct} is charge transfer resistance and Z_w is diffusion resistance.

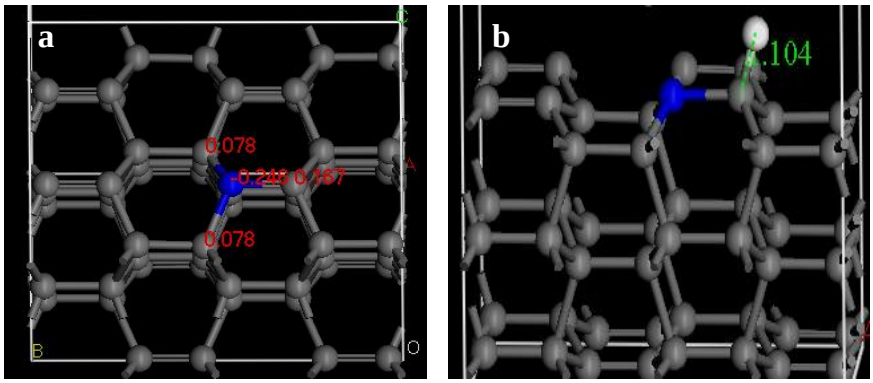

Figure S9 | Charge population and hydrogen adsorption. (a) Charge population of N and (b) hydrogen adsorption on N-doped hexagonal nanodiamond. (All calculations were performed using the Materials Studio DMol3 module. The surface of hexagonal nanodiamond (100) was modeled by a (3×2×2) supercell with 6 layers. The 3 bottom layers were fixed and the other layers were allowed to relax. In the calculations, 10 layers of vacuum were considered).

To explore the conditions for NHC preparation, the conditions for HC preparation was first determined (substrate temperature of 460 ~ 500 °C, pressure of 5.9 ~ 6.3 kPa, a gas mixture of H_2/CH_4 with CH_4 = 10 ~ 20% and deposition time of 3 ~ 5 h) and then N_2 was introduced into the gas mixture for nitrogen doping. During this process, it was found that doped nitrogen content was correlated to the

N_2 ratio in the gas mixture while the influence of temperature, pressure and deposition time was negligible when they are in the range mentioned above. The mechanism of NHC growth was proposed as follows[7-9]: when H_2 was introduced into the MPECVD system, H_2 plasma can be produced in the microwave electric filed, which dissociates the gas precursors and generates atomic hydrogen and carbon species (C_x, C_xH_y). These carbon species will nucleate on the substrate with low temperature caused by cooling water, and then grow three dimensionally until the grains coalesce, leading to the formation of a continuous polycrystalline film with grain size increasing with increased deposition time. During this process, N is doped into the carbon lattice and the temperature and pressure will influence the growth rate in different directions. Meanwhile, atomic hydrogen will each amorphous carbon and part of the graphitic carbon while diamond is stable. At last, N-doped hexagonal nanodiamond with different contents of graphitic carbon will be formed through adjusting the ratio of precursors, deposition temperature and pressure

References

1. Liu, J. *et al.* High-performance oxygen reduction electrocatalysts based on cheap carbon black, nitrogen, and trace iron. *Adv. Mater.* **25,** 6879-6883 (2013).
2. Masa, J. *et al.* Trace metal residues promote the activity of supposedly metal-free nitrogen-modified carbon catalysts for the oxygen reduction reaction. *Electrochem. Commun.* **34**, 113-116 (2013).
3. Wang, L., Ambrosi, A. & Pumera, M. Metal-free catalytic oxygen reduction reaction on heteroatom doped graphene is caused by trace metal impurities. *Angew. Chem. Int. Ed.* **52**, 13818-13821 (2013).
4. Pumera, M., Ambrosi, A. & Chng, E. L. K. Impurities in graphenes and carbon nanotubes and their influence on the redox properties. *Chem. Sci.* **3**, 3347-3355 (2012).
5. Bockris, J. O. M. & McHardy, M. J. Electrocatalysis of oxygen reduction by sodium tungsten bronze. *J. Electrochem. Soc.* **120**, 60-66 (1973).
6. Kunimatsu, K., Sato, T., Uchida, H. & Watanabe, M. Adsorption/oxidation of CO on highly dispersed Pt catalyst studied by combined electrochemical and ATR-FTIRAS methods: oxidation of CO adsorbed on carbon-supported Pt catalyst and unsupported Pt black. *Langmuir* **24**, 3590-3601 (2008).

7. Das, D. & Singh, R. N. A review of nucleation, growth and low temperature synthesis of diamond thin films. *Int. Mater. Rev.* **52**, 29-64 (2007).
8. Khaliullin, R. Z., Eshet, H. Kühne, T. D., Behler J. & Parrinello, M. Nucleation mechanism for the direct graphite-to-diamond phase transition. *Nature Mater.* **10**, 693-697 (2011).
9. Kumar, A. *et al.* Formation of nanodiamonds at near-ambient conditions via microplasma dissociation of ethanol vapour. *Nature Commun.* **4**, 1-8 (2013).